US008257991B1

(12) **United States Patent**
Park et al.

(10) **Patent No.: US 8,257,991 B1**

(45) **Date of Patent: Sep. 4, 2012**

(54) **PROCESS FOR MANUFACTURING SHELL MEMBRANE FORCE AND DEFLECTION SENSOR**

(75) Inventors: **Yong-Lae Park**, Stanford, CA (US); **Behzad Moslehi**, Los Altos, CA (US); **Richard James Black**, Menlo Park, CA (US); **Mark R. Cutkosky**, Palo Alto, CA (US); **Kelvin K. Chau**, Pleasanton, CA (US)

(73) Assignee: **Intelligent Fiber Optic Systems, Inc.**, Santa Clara, CA (US)

(*) Notice: Subject to any disclaimer, the term of this patent is extended or adjusted under 35 U.S.C. 154(b) by 0 days.

(21) Appl. No.: **13/042,168**

(22) Filed: **Mar. 7, 2011**

Related U.S. Application Data

(63) Continuation of application No. 12/100,417, filed on Apr. 10, 2008, now Pat. No. 7,903,907.

(51) **Int. Cl.**
H01L 21/00 (2006.01)
G02B 6/00 (2006.01)
G01J 1/04 (2006.01)
G01L 19/04 (2006.01)

(52) **U.S. Cl.** **438/31**; 438/29; 385/12; 385/13; 385/100; 385/31; 385/37; 250/227.11; 250/227.14; 73/708; 264/1.24; 264/1.25; 264/1.27

(58) **Field of Classification Search** 385/12, 385/13, 37, 31, 100, 123; 250/227.11, 227.14, 250/227.18, 227.23; 73/1.37, 1.71, 61, 67, 73/705, 744, 708; 438/29, 31; 264/1.24, 264/1.25, 1.27, 1.29, 1.7, 2.5
See application file for complete search history.

(56) **References Cited**

U.S. PATENT DOCUMENTS

4,678,903	A	*	7/1987	Wlodarczyk et al.	250/227.14
4,729,627	A	*	3/1988	Saito et al.	385/13
4,733,068	A	*	3/1988	Thiele et al.	250/227.14
4,932,262	A		6/1990	Wlodarczyk	
5,005,584	A		4/1991	Little	
5,425,273	A	*	6/1995	Chevalier	73/705
5,633,494	A	*	5/1997	Danisch	250/227.16
5,825,489	A		10/1998	Lagakos et al.	
6,080,982	A	*	6/2000	Cohen	250/227.11
6,160,762	A	*	12/2000	Luscombe et al.	367/149
6,233,374	B1	*	5/2001	Ogle et al.	385/13
6,278,811	B1	*	8/2001	Hay et al.	385/13
6,422,084	B1		7/2002	Fernald et al.	
6,439,055	B1	*	8/2002	Maron et al.	73/705
6,452,667	B1	*	9/2002	Fernald et al.	356/73.1
6,559,437	B1	*	5/2003	Pope et al.	250/227.14
6,626,043	B1	*	9/2003	Bailey et al.	73/705
6,774,354	B2	*	8/2004	Ames	250/227.14
6,785,443	B2	*	8/2004	Mendez et al.	385/37

(Continued)

Primary Examiner — Brian Healy

(74) *Attorney, Agent, or Firm* — File-EE-Patents.com; Jay A. Chesavage

(57) **ABSTRACT**

A sensor for force is formed from an elastomeric cylinder having a region with apertures. The apertures have passageways formed between them, and an optical fiber is introduced into these passageways, where the optical fiber has a grating for measurement of tension positioned in the passageways between apertures. Optionally, a temperature measurement sensor is placed in or around the elastomer for temperature correction, and if required, a copper film may be deposited in the elastomer for reduced sensitivity to spot temperature variations in the elastomer near the sensors.

21 Claims, 12 Drawing Sheets

Sensor with elastomeric shell

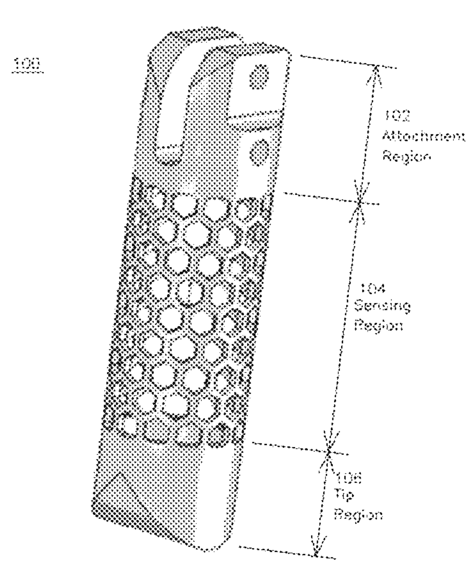

U.S. PATENT DOCUMENTS

6,813,013	B2	11/2004	Fernald et al.	
6,820,489	B2 *	11/2004	Fernald et al.	73/705
6,959,604	B2	11/2005	Bryant et al.	
7,047,816	B2	5/2006	Jones et al.	
7,155,074	B2	12/2006	Kersey	
7,266,261	B2	9/2007	Arias Vidal et al.	
7,308,165	B2	12/2007	Arias Vidal et al.	
7,315,666	B2 *	1/2008	Van Der Spek	385/12
7,447,390	B2	11/2008	Dunphy et al.	
7,458,273	B2	12/2008	Skinner et al.	
7,520,176	B1	4/2009	Ko et al.	
7,903,907	B1 *	3/2011	Park et al.	385/12
2004/0082844	A1 *	4/2004	Vardi et al.	600/407
2006/0071158	A1 *	4/2006	Van Der Spek	250/227.14

* cited by examiner

Figure 1

Sensor with elastomeric shell

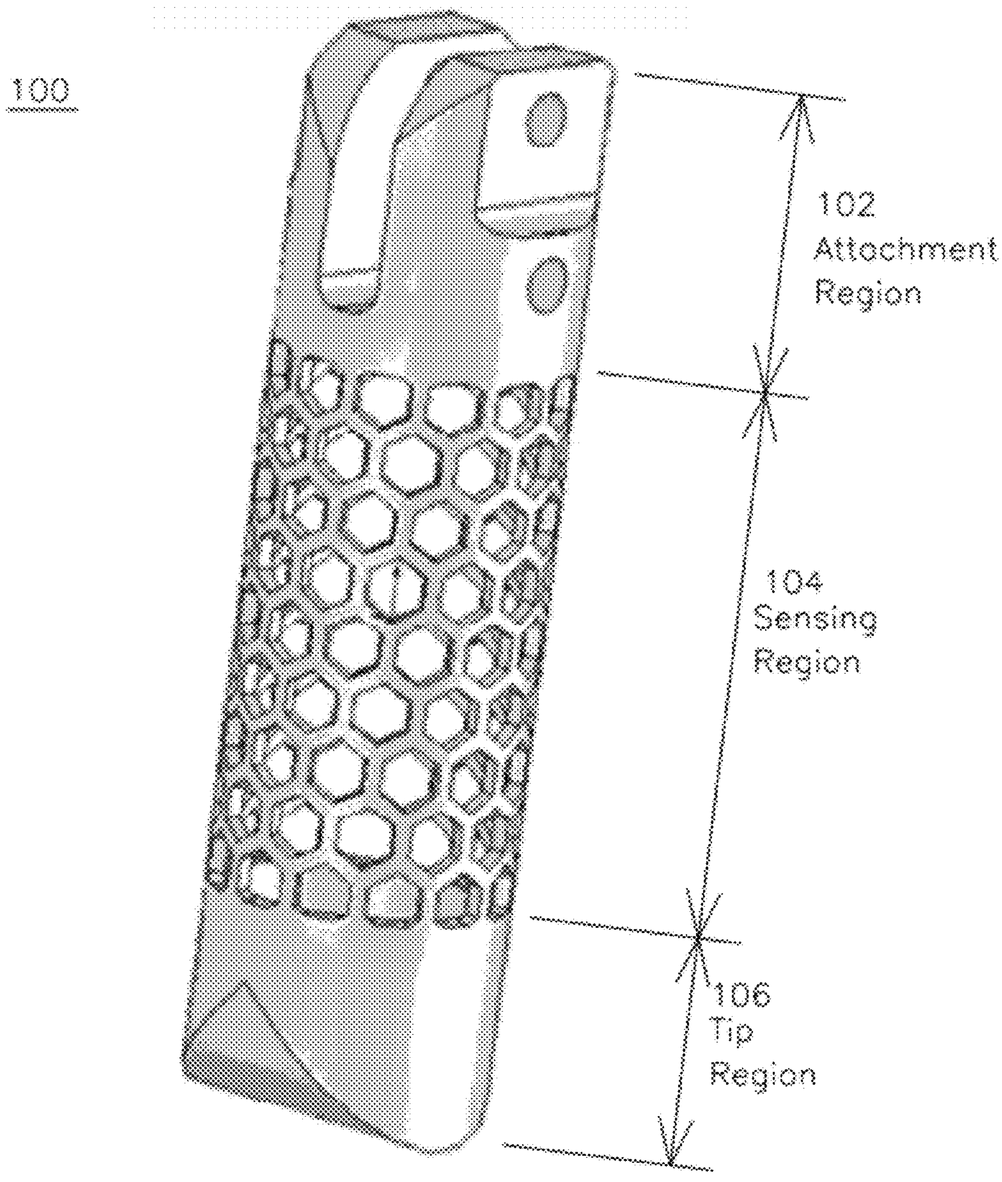

Figure 2A

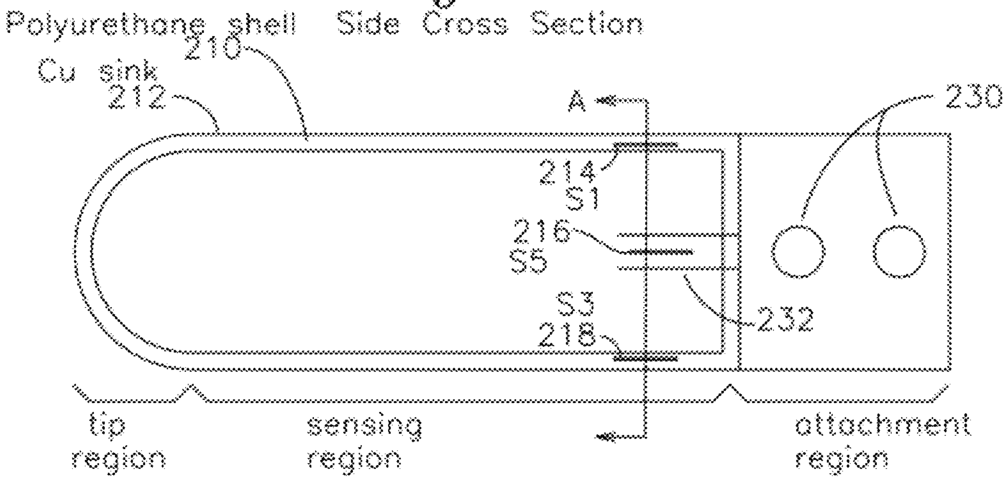

Figure 2B

Section A-A

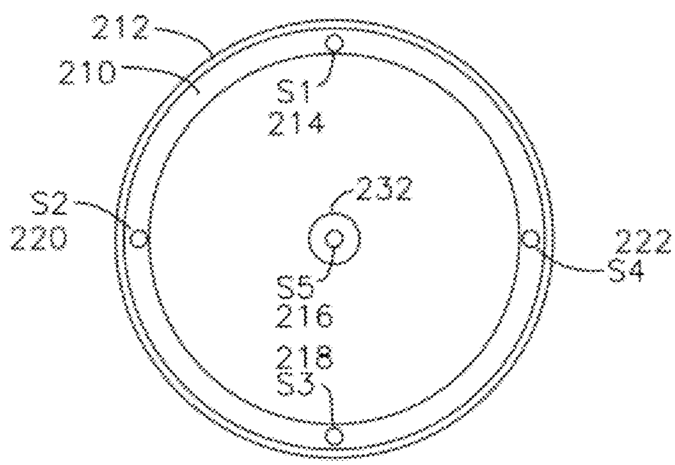

Deflection, force applied at end

Figure 3A Front view

Figure 3B Side view

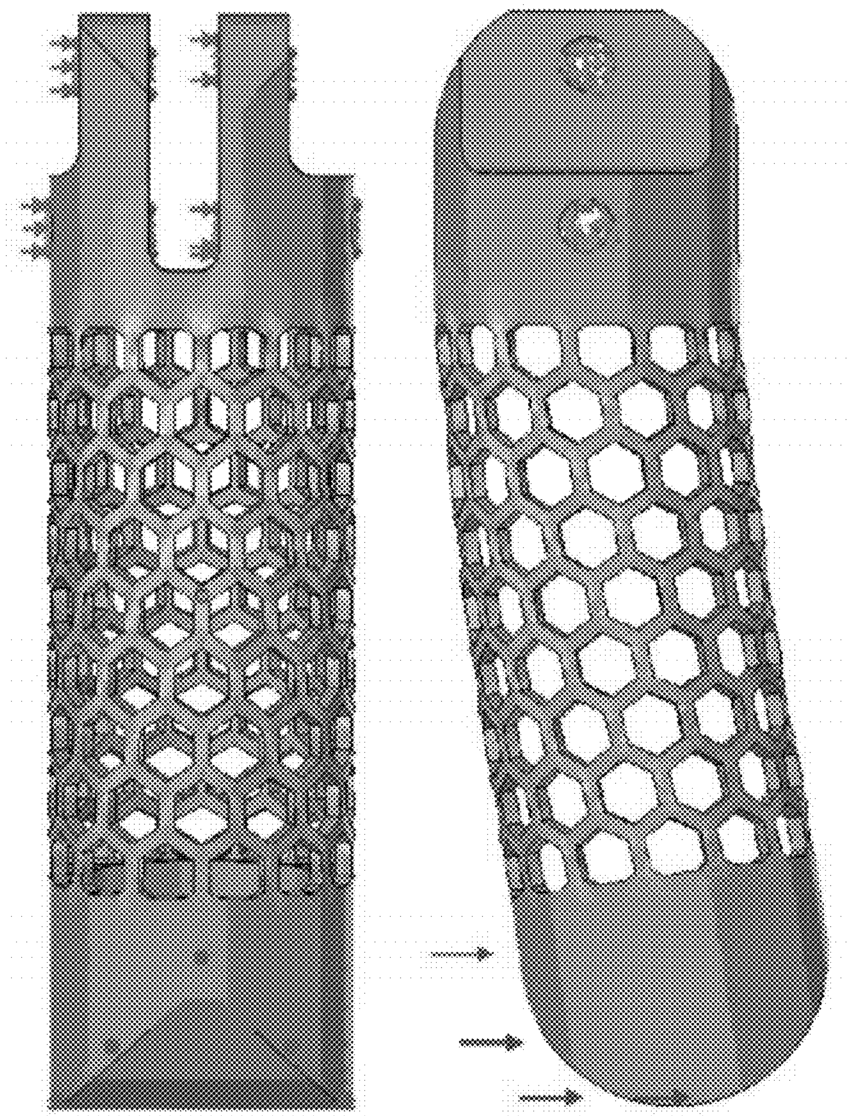

Deflection, force applied at lattice

Figure 3C
Front view

Figure 3D
Side view

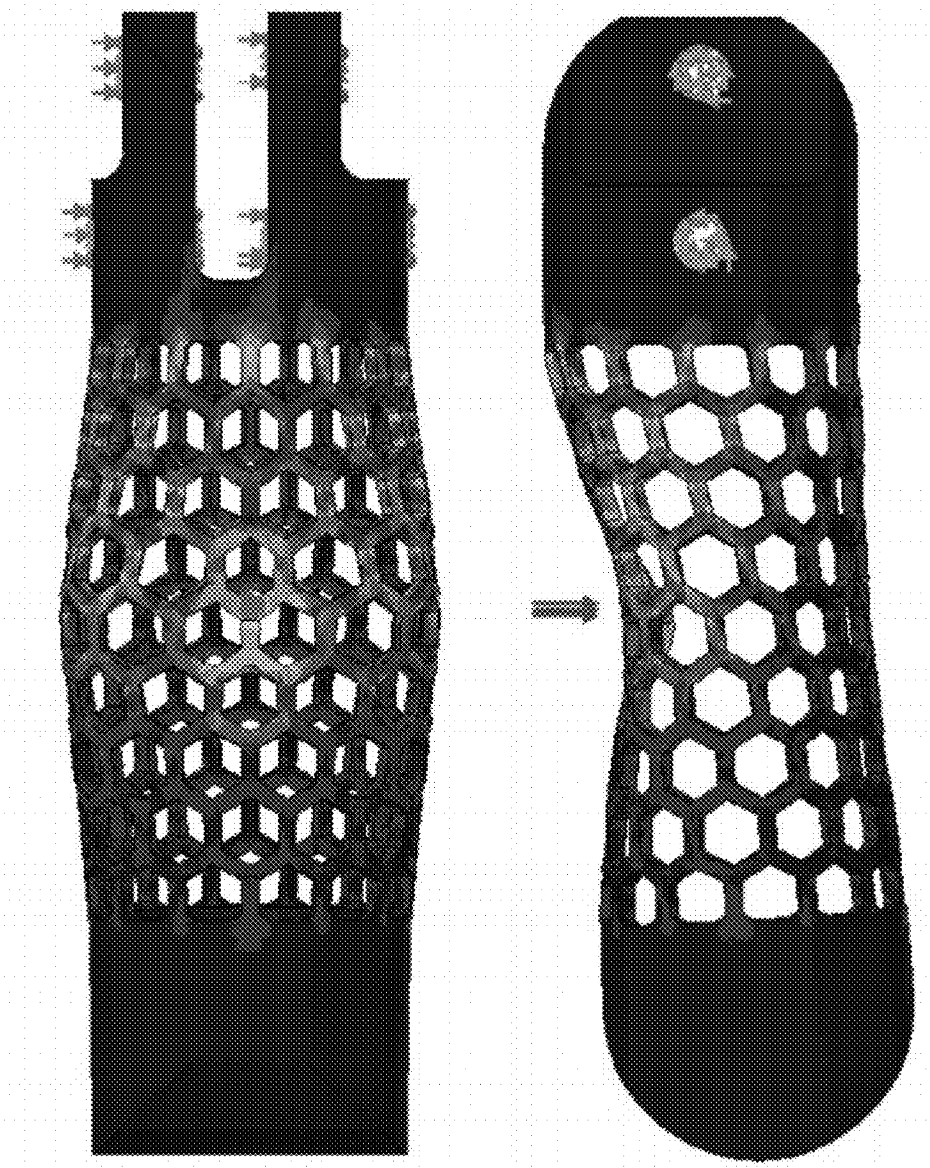

Figure 4A *Figure 4B* *Figure 4C*

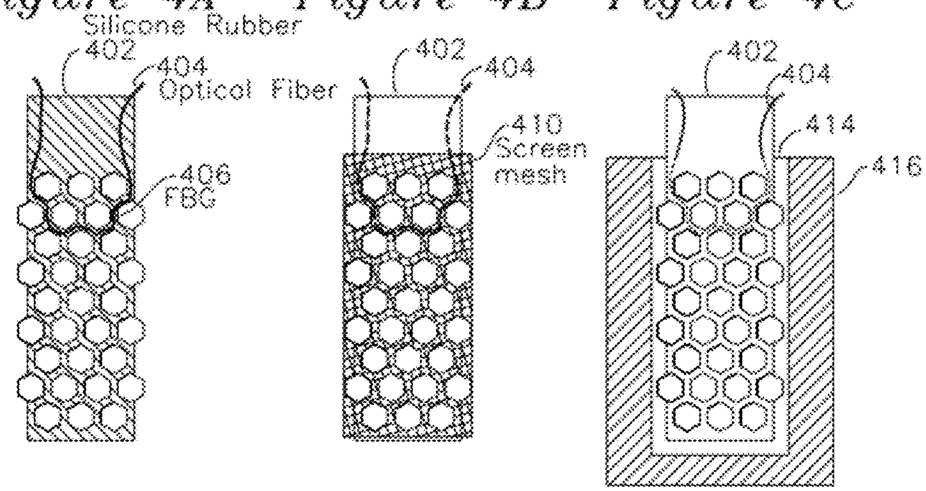

Figure 4D *Figure 4E* *Figure 4F*

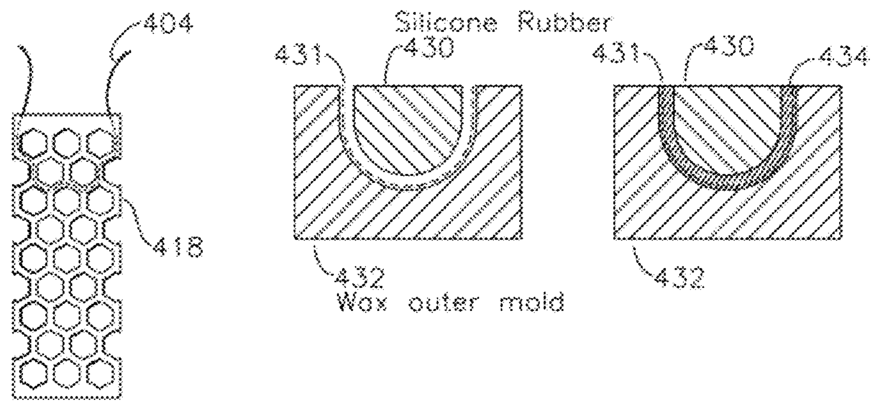

Figure 4G

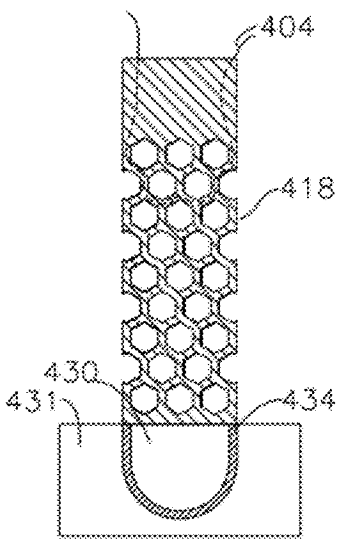

Figure 4H

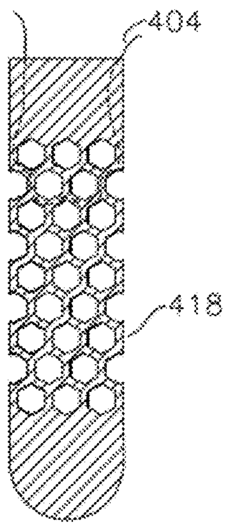

Figure 4I

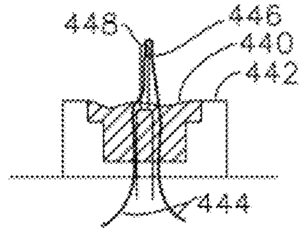

Figure 4J

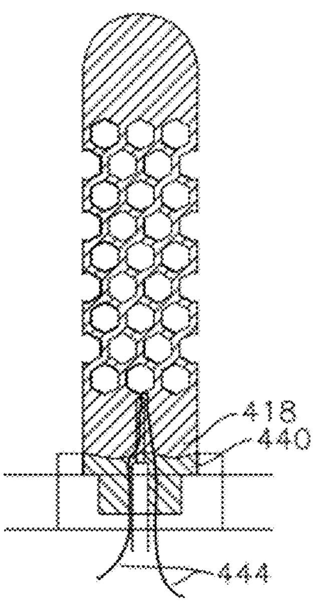

Figure 4K

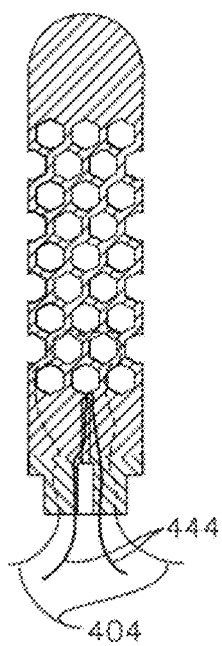

Figure 5A

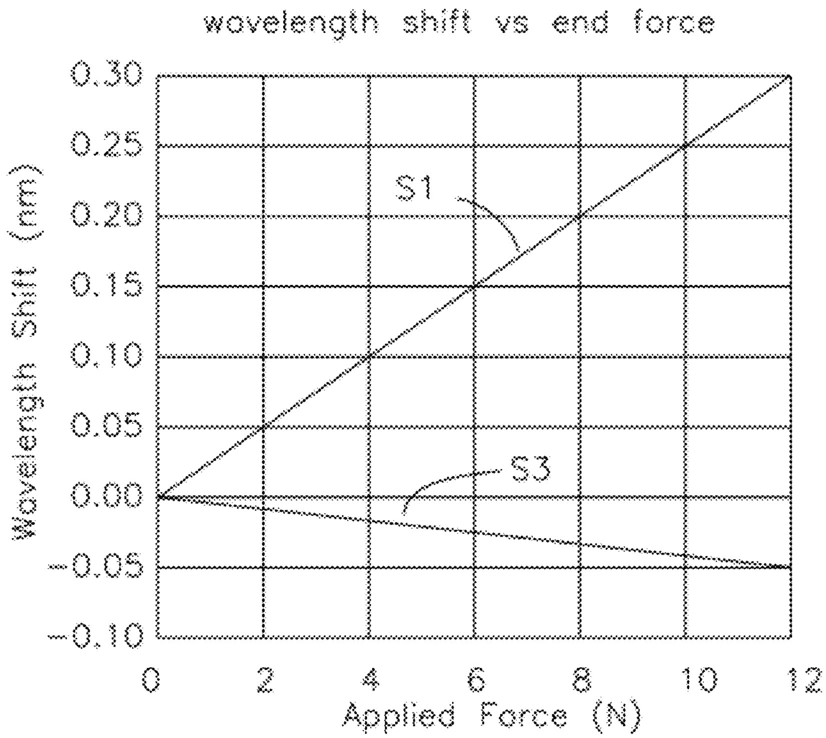

Figure 5B

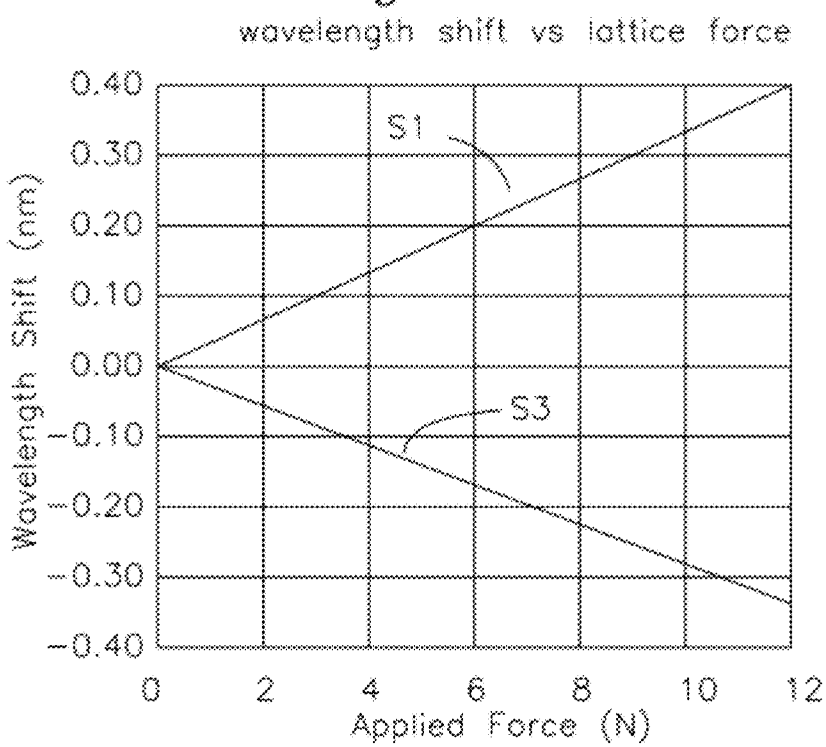

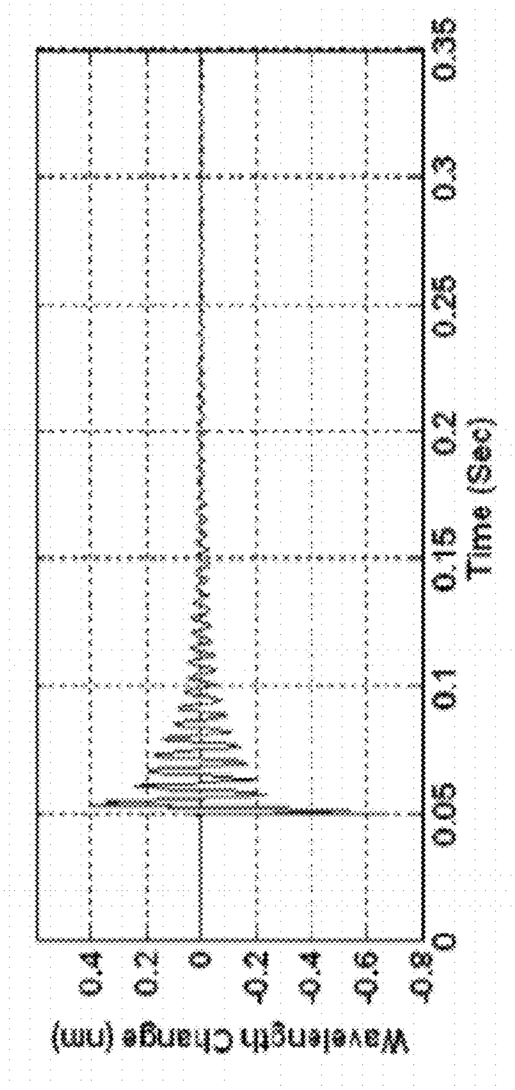

Figure 6A

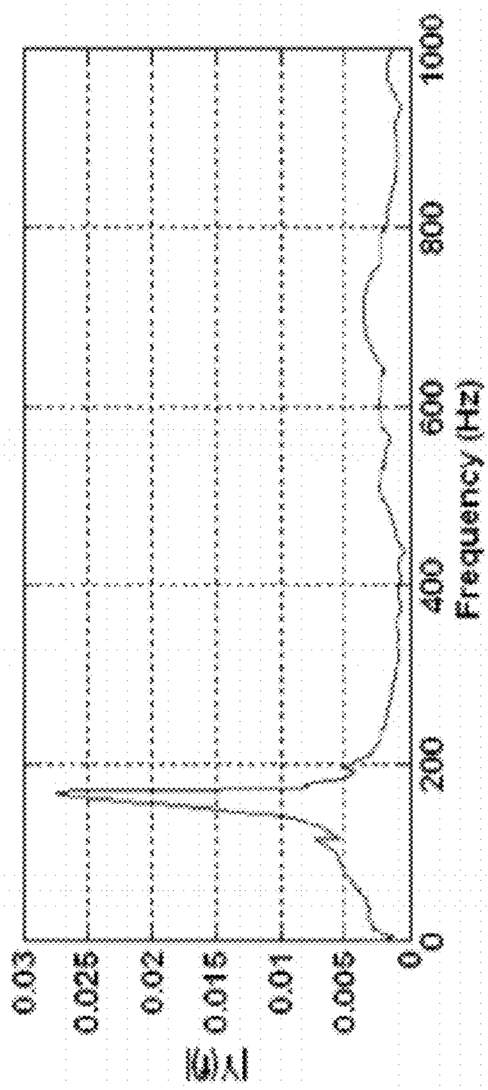

Figure 6B

Figure 7

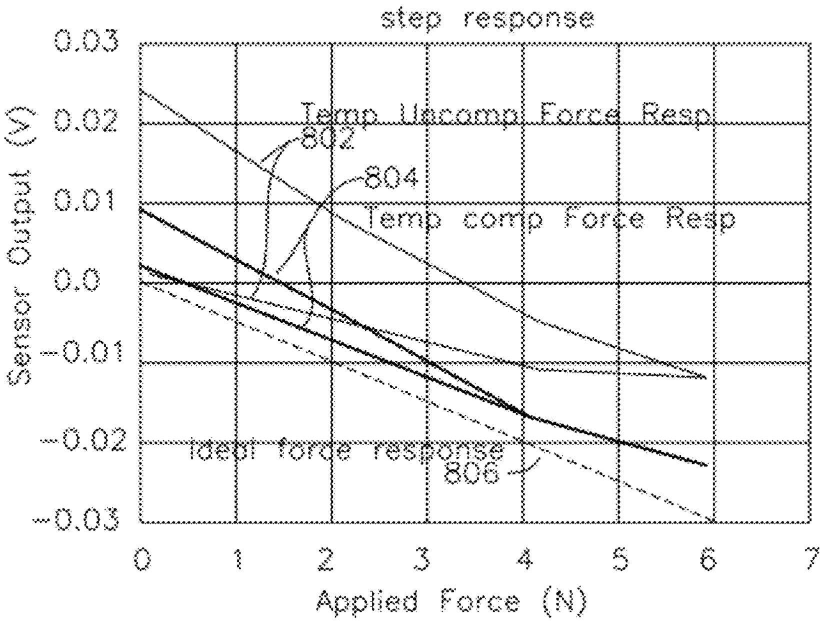

Figure 9

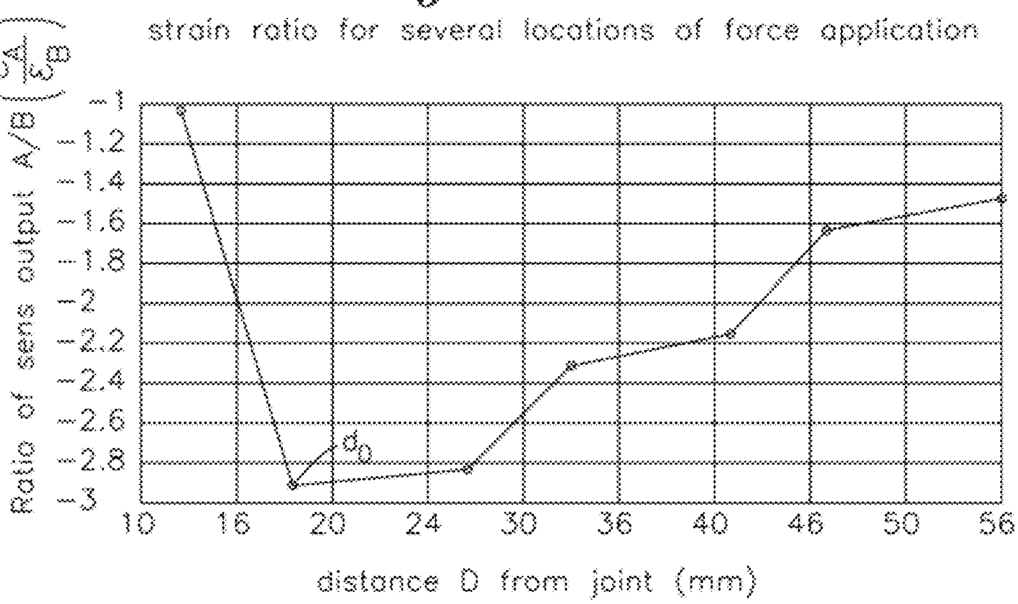

Figure 8A

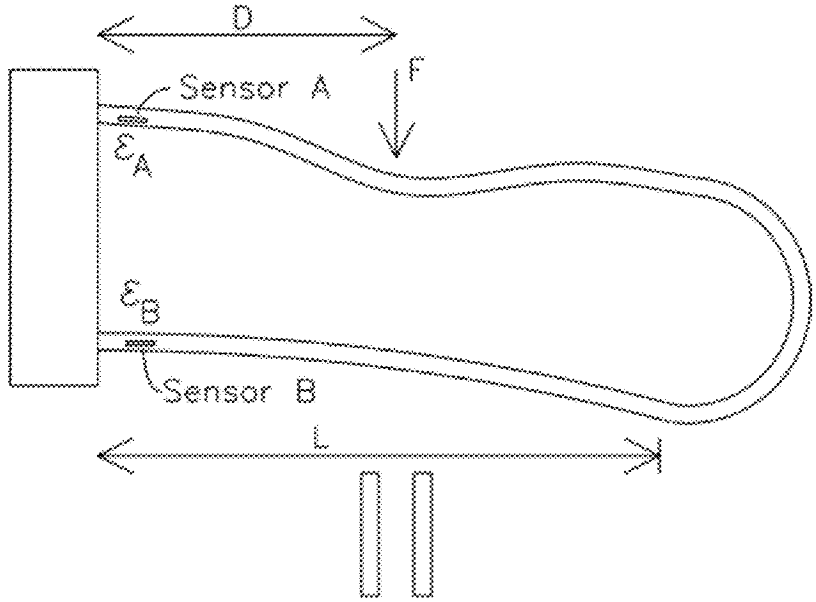

Figure 8B

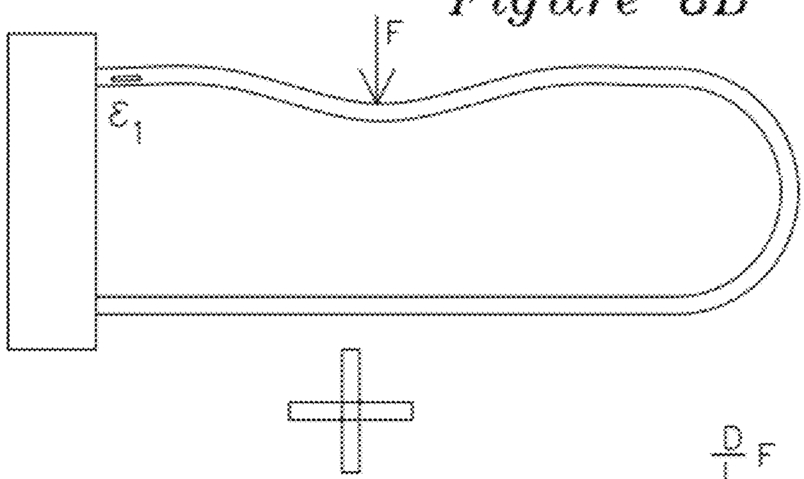

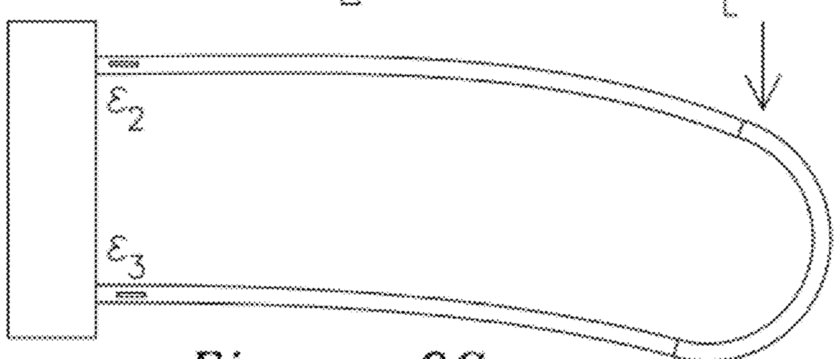

Figure 8C

Figure 10

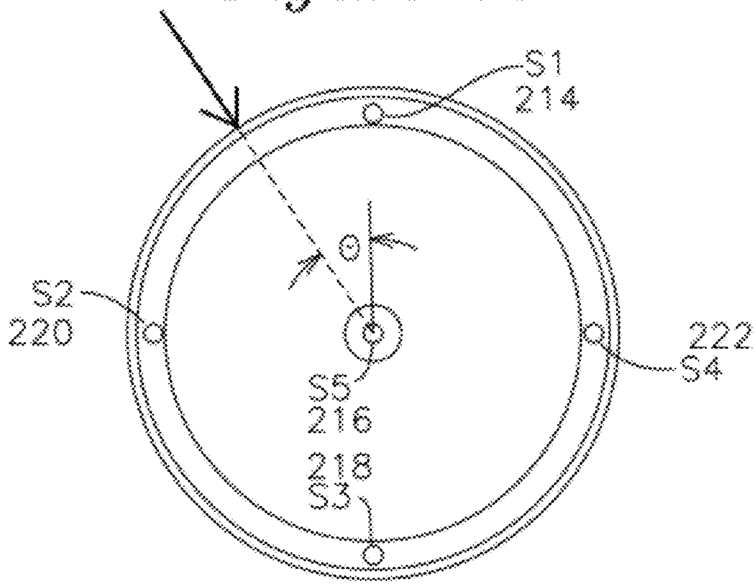

Figure 11

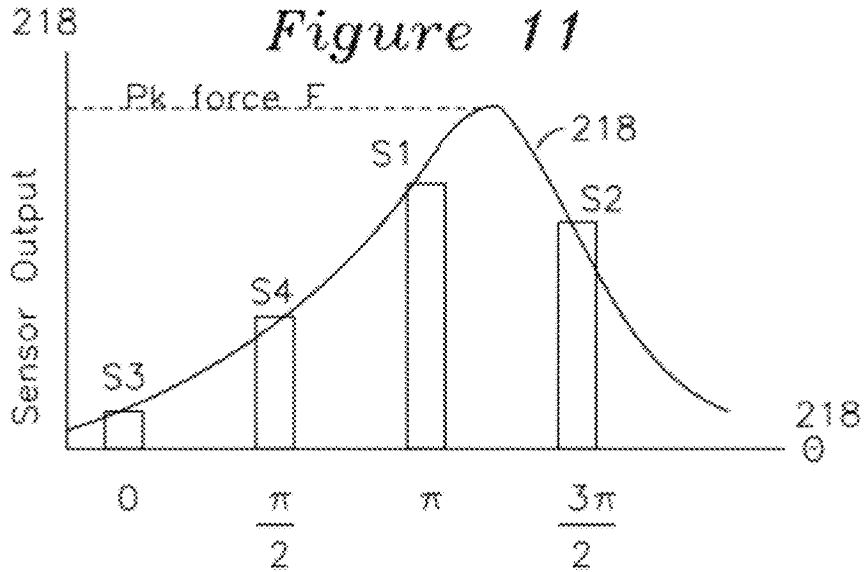

Figure 12

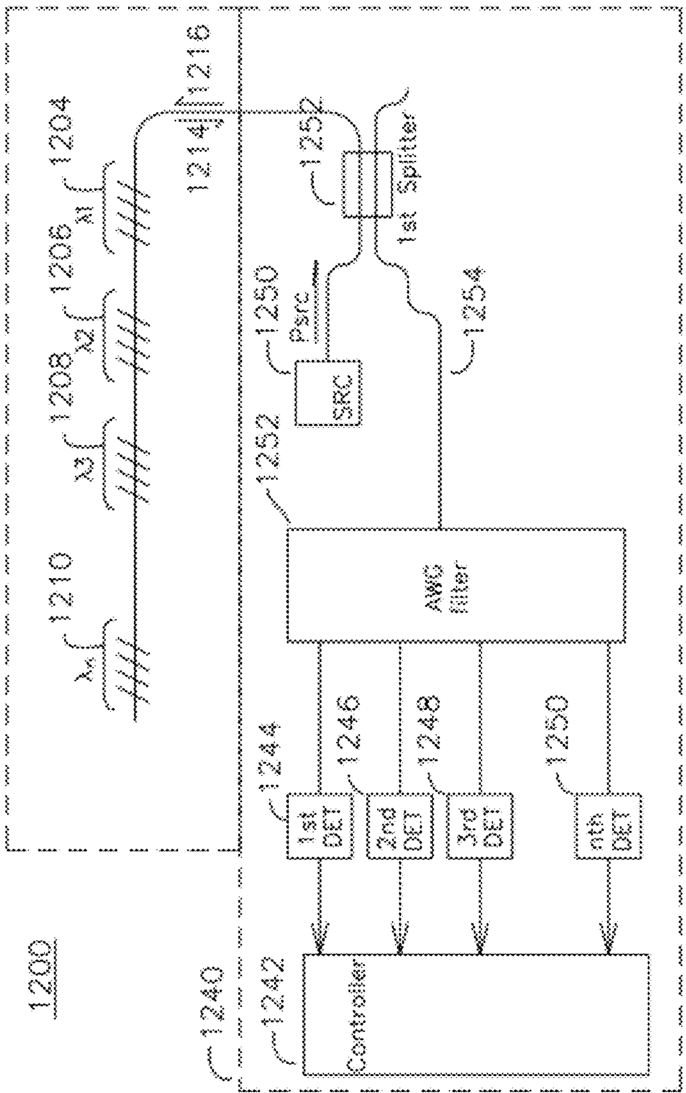
1200
1202
1204
1206
1208
1210
λ1
λ2
λ3
1214
1216
1252
1250
Psrc
SRC
1st Splitter
1254
AWG filter
1244
1246
1248
1250
1st DET
2nd DET
3rd DET
nth DET
1240
1242
Controller

PROCESS FOR MANUFACTURING SHELL MEMBRANE FORCE AND DEFLECTION SENSOR

The present patent application is a continuation of Ser. No. 12/100,417 filed Apr. 10, 2008, now issued as U.S. Pat. No. 7,903,907.

The present invention was developed under National Aeronautics and Space Administration (NASA) Contracts #NNJ05JC02C and NNJ06JA36C. The government has certain rights in this invention.

BACKGROUND OF THE INVENTION

1. Field of the Invention

The present invention relates to a force and deflection sensor. In particular, the invention relates to an flexible shell formed with an elastomer having passageways formed by apertures in the shell, with an optical fiber having one or more Bragg gratings positioned in the passageways for the measurement of force and deflection.

2. Description of the Related Art

Future robots are expected to free human operators from difficult and dangerous tasks requiring high dexterity in various environments. One example is an extra-vehicular repair of a manned spacecraft that would otherwise require hazardous work by human astronauts. Another example is robotic surgery in which accurate manipulation is crucial. Operating complicated tools and performing delicate tasks require a manipulator of great precision and coordination. Therefore, force sensing is one of the most critical requirements for this type of robot control. Typically, robots have a modest number of mechanical sensors, often associated with actuators or concentrated in a special device such as a force sensing wrist. As a result, robots often poorly identify and respond to unexpected and arbitrarily-located impacts.

One object of the invention is a light-weight, rugged appendages for a robot that features embedded sensors so that the robot can be more aware of both anticipated and unanticipated loads in real time. A particular class of optical sensors, Fiber Bragg Grating (FBG) sensors, is promising for space robotics and other applications where high sensitivity, multiplexing capability, immunity to electromagnetic noise, small size and resistance to harsh environments are particularly desirable. In addition, the biosafe and inert nature of optical fibers making them attractive for medical robotics. FBGs reflect light with a peak wavelength that shifts in proportion to the strain to which they are subjected. This wavelength shift provides the basis for strain sensing with typical values for the sensitivity to an axial strain being approximately 1.2 pm/microstrain at 1550 nm center wavelength. In combination with a prior art FBG interrogator, submicrostrain resolution measurements are possible. In addition, the strain response is linear with no indication of hysteresis at temperatures as high as 370° C. and, with appropriate processing, to over 650° C. Multiple FBG sensors can be placed along a single fiber and optically multiplexed. FBG sensors have previously been surface attached to or embedded in metal parts and composites to monitor stresses.

SUMMARY OF THE INVENTION

A sensor is formed from a thin shell of flexible material such as elastomer to form an attachment region, a sensing region, and a tip region. In one embodiment, the sensing region is a substantially cylindrical flexible shell and has a plurality of apertures forming passageways between the apertures. Optical fiber is routed through the passageways, with sensors located in the passageways prior to the application of the elastomeric material forming the flexible shell. Deflection of the sensor, such as by a force applied to the contact region, causes an incremental strain in one or more passageways where the optical fiber is located. The incremental strain results in a change of optical wavelength of reflection or transmittance at the sensor, thereby allowing the measurement of force or displacement.

BRIEF DESCRIPTION OF THE DRAWINGS

FIG. **1** is a perspective view of an elastomeric sensor.

FIG. **2**A is a cross section view of a sensor.

FIG. **2**B is a section view of the sensor of FIG. **2**A

FIG. **3**A is a front view of a sensor with a force applied to the tip.

FIG. **3**B is a side view of a sensor with a force applied to the tip.

FIG. **3**C is a front view of a sensor with a force applied to a sensing region.

FIG. **3**D is a side view of a sensor with a force applied to a sensing region.

FIGS. **4**A, **4**B, **4**C, **4**D, **4**E, **4**F, **4**G, **4**H, **4**I, **4**J, **4**K show process steps for forming an elastomeric sensor.

FIGS. **5**A and **5**B are plots of wavelength shift vs. applied force.

FIGS. **6**A and **6**B are plots of dynamic impulse response and its fast Fourier transform.

FIG. **7** is a plot of force measurement accuracy for temperature compensated and temperature uncompensated configurations.

FIG. **8**A is a cross section view of deformation at the sensor region.

FIGS. **8**B and **8**C are superposition views of the force-induced deformation of FIG. **8**A.

FIG. **9** is a plot of a strain ratio versus applied force along various points from the sensor joint.

FIG. **10** is a top view of a sensor at a region of applied force.

FIG. **11** is a plot of sensor output for the sensors of FIG. **10**.

FIG. **12** is a block diagram for a wavelength discriminator coupled to a series connection of FBGs.

DETAILED DESCRIPTION

FIG. **1** shows a perspective view of an example embodiment of a sensor finger **100** having an attachment region **102**, a hollow sensing region **104**, and a hollow tip region **106**. The sensor is not limited in its dimensions, but in one example embodiment, the attachment region extent is approximately 35 mm, the sensing region extent is approximately 65 mm, and the tip region extent is approximately 20 mm with a cylindrical diameter of 35 mm. FIG. **2**A shows a simplified cross section view of the sensor of FIG. **1**, which includes a polyurethane shell **210** forming the tip region and sensing region, transitioning to a rigid attachment region including mounting holes **230**. The shell **210** has a fiber optic cable embedded in it, which may route through passageways of the sensing region and tip region in any manner through the shell **210**, and having a plurality of strain sensors formed as Bragg gratings in particular regions such as **214** and **218** of the shell **210**. FIG. **2**B shows a section A-A of FIG. **2**A, including four such strain sensors **S1 214**, **S3 218**, **S2 220**, and **S4 222**. A control sensor **S5 215** is positioned at the center, and is not exposed to strain, but measures temperature for use in compensating temperature effects from strain sensors **S1**, **S2**, **S3**, **S4**.

The exoskeletal structure of the shell **210** is light weight while maintaining relatively high strength. Since the sensing region structure deforms not only locally but globally depending on the location of force application, the sensor finger **100** is able to measure and localize applied forces. This is useful for both grasp force measurement and collision detection.

In one embodiment of the invention, the sensing region **104** has a hexagonally patterned shell. This pattern allows the structure to concentrate stresses and strains on the narrow ribs, facilitates embedded sensor placement and has an added effect of amplifying the sensor signal. Although two other regular polygons, triangles and squares, can also be used exclusively to form the shell pattern, the hexagon minimizes the ratio of perimeter to area. In addition, the hexagonal cells avoid sharp interior corners which could reduce the fatigue life. In summary, the hexagonal structure can minimize the amount of material for fabrication and the weight of the part while providing high structural strength. Although shown as a regular array of hexagonal aperture patterns, the sensor passageways could be formed many different ways and with various combinations of apertures, including pairs of apertures with a sensor placed therebetween, an array of sensors with circular symmetry, radial symmetry, or circumferential symmetry, and the passageways containing the sensors may have any orientation with respect to the axis of the sensing region **104**.

Polymer structures unavoidably experience greater creep than metal structures. Creep adversely affects the linearity and repeatability of the embedded sensor output, both of which are mainly dependent on the stiffness and resilience of the structure. In addition, thermal changes can affect the FBG strain sensor outputs. A copper mesh **212** can be embedded into the outside of the shell, to reduce creep and provide thermal shielding. The high conductivity of copper expedites distribution of heat applied from outside the shell and creates a more uniform temperature gradient inside the shell.

Additional sensors provide more information and make the system more reliable. In an example embodiment, the force information obtained from the system includes longitudinal location, latitudinal location, magnitude of applied force, and orientation of the force vector. For simplicity, it will be assumed that forces are applied only in a normal direction to the surface. Since this assumption reduces the number of unknowns to three, a minimum of three linearly independent sensors are needed. In the present example, four strain sensors are embedded in the shell. Optimal sensor locations may be determined through the use of finite element analysis of the sensor shell. FIG. **3** shows strain distributions when different types of forces are applied to the shell and to the fingertip. Strain is most concentrated at the top of the shell where it is connected to the joint. Therefore, four sensors were embedded at 90° intervals into the first rib of the shell, closest to the joint, as shown in FIG. **2**B, which also shows the center reference temperature sensor S**5** **216**, which may be partially enclosed in a shielding cylinder **232** such as stiff copper or other structure to minimize short-term effects such as air currents.

Since embedded FBG sensors are sensitive to temperature change as well as strain change, it is necessary to isolate thermal effects from mechanical strains. Among the temperature compensation methods available are the dual-wavelength superimposed FBG sensors, saturated chirped FBG sensors, and an FBG sensor rosette. In contrast, a simpler method shown in the present example embodiment is the use of an isolated, strain-free FBG sensor S**5** **216** to directly measure the thermal effects. Subtracting the wavelength shift of this temperature-compensation sensor from that of any other sensor corrects for the thermal effects on the latter. An important assumption in this method is that all sensors are at the same temperature. The example embodiment of FIGS. **2**A and **2**B shows one temperature compensation sensor S**5** **216** in the hollow area in the middle of the shell **210** as shown in FIG. **2**. Although the temperature compensation sensor S**5** **216** is physically removed from the strain sensors, the copper heat shield **232** is expected to create a more uniform temperature gradient inside the shell.

FIGS. **4**A, **4**B, **4**C, **4**D, **4**E, **4**F, **4**G, **4**H, **4**I, **4**J, and **4**K shows the sequence of steps of a modified SDM process for prototype fabrication, which may be examined in combination with the below process steps:

Shell (Sensor Region) Part Fabrication:

FIG. **4**A shows the preparation of a silicone rubber inner mold **402** with optical fiber **404** with FBG sensor **406** placed with the FBG sensors **406** in desired measurement passageways formed in the mold. Typically, multiple FBGs operating at the same or different wavelengths are employed on a single fiber, although only one is shown for clarity.

FIG. **4**B shows the inner mold **402** with optical fiber **404** wrapped with copper screen mesh **410**. In one embodiment of the invention, the screen mesh has a matching hole pattern for the apertures formed as pedestals into inner mold **402**, and the pedestals may also have a formed lip to support the mesh **410** at a desired height above the cylindrical inner diameter of the inner form **402**.

FIG. **4**C shows a form void **414** produced by the gap between the inner mold **402** which has the screen **410** applied, and the outer form **416**. Liquid polyurethane is then poured into the form gap **414**.

FIG. **4**D shows the formed sensing region **418** after curing of the polyurethane and removal of the inner and outer molds with embedded optical fiber **404** and copper mesh (not shown).

[Step **2**] Tip Region Part Fabrication

FIG. **4**E shows the preparation of the silicone rubber inner mold **430** and wax outer mold **432** with the copper mesh placed in the form void **431**.

FIG. **4**F shows the liquid polyurethane poured into the form void **431** produced by the inner **430** and outer 432 molds.

FIG. **4**G shows the placement of the cured sensing region **418** from Step **1** into the uncured polyurethane void **434** of the tip region mold, thereby joining the formed sensing region **418** with the tip region.

FIG. **4**H shows the tip and sensor regions after removal from the mold with the polyurethane cured, including strain sensor fiber **404**.

[Step **3**] Attachment Region Part Fabrication

FIG. **4**I shows the preparation of the outer mold with the placement of the temperature compensation sensor structure including measurement fiber **444** with grating **446** located in shield cylinder **448**, all of which is placed in base mold **442** with liquid polyurethane **440**.

FIG. **4**J shows the cured shell and fingertip parts placed into the uncured polyurethane.

FIG. **4**K shows the completed sensor after removal of the outer mold when the polyurethane cures, including temperature measurement fiber **444** and strain measurement fiber **404**.

The series of FIGS. **4**A through **4**F show just one embodiment for the steps of the Shape Deposition Manufacturing (SDM) process for the finger prototype fabrication. As is known in the prior art, it is difficult to make hollow three-dimensional parts using conventional SDM processes, since only the top of the part is accessible for machining. The outer mold **431** and **416** may be formed from hard wax to maintain the overall shape. In contrast, the inner mold **402** can be hollow and made of soft silicone rubber, which can be manually deformed and removed when the polyurethane is cured. The strain sensors and copper mesh can be embedded during these steps. The second series of steps is related to fingertip casting, which uses a separate mold and occurs after the shell **418** is fully cured. As it cures, the polyurethane for the fingertip **434** bonds to the cured polyurethane of the shell **418**. In the final step, the attachment joint including temperature compensation structure **446** and **448** are cast. As with the fingertip, the joint bonds to the cured shell. Since the joint is not hollow, an inner mold is not needed during this step. Since the joint has no copper mesh, it was cast using a hard polyurethane (such as Task 9, Smooth-On, Easton, Pa., USA) to reduce creep, while the shell and fingertip can be cast from softer polyurethane (such as Task 3, Smooth-On, Easton, Pa., USA).

To evaluate the resulting structure, three different sets of tests were carried out to evaluate the static, dynamic, and thermal performance of the prototype. The static tests show how linear and repeatable the system is, the dynamic tests show how responsive the system is, and the thermal tests show how well the system compensates for errors caused by temperature change.

Static Tests Static forces were applied to two different locations on the finger: lattice shell region **104** and tip region **106**. FIGS. **5**A and **5**B show the responses of two of the four sensors for a normal force applied in the sensing region and tip region, respectively. Applying a force to the shell yielded sensitivities of 0.024 nm/N and −0.0044 nm/N for sensor **51** and S**3**, respectively. The optical system can resolve wavelength changes of 0.5 pm or less, corresponding to 0.015 N or less for the minimum detectable force change. Note that the 51 sensor, being on the same side of the shell as the contact force, has a much higher sensitivity to it. Applying a force to the tip yielded sensitivities of 0.032 nm/N and −0.029 nm/N. In this case, the location of the force results in roughly equal strains at both sensors. For a given location, the ratio of the two sensor outputs is independent of the magnitude of the applied force. The plots of FIGS. **5**A and **5**B shows a maximum of 5.3% and 3.9% deviations from linear responses for shell and tip tests, respectively.

Characterization of the dynamic response of the sensorized fingers can be seen in FIGS. **6**A and **6**B, which show the impulse response (expressed as a change in the wavelength of light reflected by an FBG cell) and its fast Fourier transform (FFT). The impulse was effected by tapping on the finger with a light and stiff object. The FFT shows a dominant frequency around 167 Hz which is a result of the dominant vibration mode of the elastomer structure.

FIG. **7** shows a typical thermal test results. Over a three minute period, the fingertip was loaded and unloaded while the temperature was decreased from 28.3 C to 25.7 C. The ideal (temperature invariant) sensor output is indicated by the dashed line **806**. Experiment results show that use of the temperature compensation sensor of plot **804** reduces thermal effects, compared to the uncompensated plot **802**.

Longitudinal localization requires some understanding of structural deformation of the shell. FIG. **8**A shows simplified two-dimensional diagrams of one embodiment of the invention. When a force is exerted at a certain location, as shown in FIG. **8**A, the structure will deform and sensors A and B will measure strains ϵ_A and ϵ_B, respectively as indicated. This situation can be decomposed into two separate effects, as shown in FIGS. **8**B and **8**C. By superposition, $\epsilon_A=\epsilon_1+\epsilon_2$ and $\epsilon_B=\epsilon_3$. Therefore, if the ratio of ϵ_A to ϵ_A is known, it is possible to estimate D, the longitudinal location of the force. FIG. **9** shows the plot of experimental ratios of ϵ_A to ϵ_B as a function of D. There is some ambiguity in the localization, since two values of D result in the same ratio. However, if we let d**0** be the distance at which ϵ_A/ϵ_B is minimized, and we restrict operation to the region d>d**0**, the ambiguity can be resolved. Further, if the sensor locations are positioned closer to the other surface of the shell, d**0** approaches 0 and it is possible to localize an applied force closer to the joint.

Latitudinal location can be approximated using centroid and peak detection, and only one point contact force is assumed in this method. FIG. **10** shows a cross sectional view of the finger with four strain sensors and an applied contact force indicated, and FIG. **11** shows its corresponding sensor signal outputs. The two sensors closest to the force location will experience positive strains (positive sensor output), and the other two sensors negative strains (negative sensor output), regardless of the longitudinal location of the force, if d>d**0**. However, since all the sensor signals must be non-negative to use the centroid method, all signal values must have the minimum signal value subtracted from them. Then, it is possible to find the angular orientation ⊖ of the contact force:

$$\theta = \frac{\Sigma\phi_i S_i'}{\Sigma S_i'} - \alpha$$

for i=1, 2, 3, 4, where S'=Si−min{S**1**,S**2**,S**3**,S**4**}, ϕ**1**=α, and $\phi_k=\phi_{k-1}+\pi/2$, for k=2, 3, 4 (if $\phi_k \geqq 2\pi$, $\phi_k=\phi_k-2\pi$), Si is the output signal from sensor i, and α is the clockwise angle between sensor **1** and the sensor with the minimum output signal value. This method produced errors less than 2°, corresponding to less than 0.5 mm on the perimeter, and an offset of 1.5° in the FEM simulation.

The FBG sensors can be interrogated using a system such as IFOS I*Sense, described in U.S. Pat. Nos. 7,127,132, 6,895,132, 6,788,835, 6,751,367, and 6,597,822, which are incorporated herein by reference. This type of interrogator relies on parallel photonic processing whereby multiple sensors are placed in series on a single fiber, which in combination with the ability to place sensors over the many channels of the sensor **100**, has the near-term potential to combine high channel counts (>100 sensors on a single fiber), high resolution (sub-microstrain), and high speed (>5 kHz) with a miniaturized footprint. As previously discussed, the application of strain on each FBG produces a shift in the wavelength that is linearly proportional to the strain. An FBG interrogator is used to precisely measure, for each FBG, the reflected wavelength shift and thus the strain applied to that FBG. Interrogators can be tunable (examining each FBG sequentially) or parallel processing in nature—the latter approach, which forms the basis of the preferred interrogator system, has advantages in terms of speed particularly when dealing with many sensors.

One example of a fiber interrogation system is shown in FIG. **12**. A broadband source **1250** sends light through the optical circulator or splitter **1252** to an array of series FBGs **1202**, each of which **1204**, **1206**, **1208**, **1210** reflects a different Bragg wavelength. The reflected light **1214** is then returned through the optical circulator **1252** to the photonic processor which both demultiplexes the light using AWG filter **1252** coupled to detectors **1244** through **1250** and provides the basis for a ratiometric approach to measuring each of the returned wavelengths through conversion to different signals in various outputs from the multi-channel photodetector array. A controller **1242** containing electronics and software compares the ratios of optical stimulation across the detectors to provide the final conversion of the arrayed signals to wavelength and eventually the strain to which each FBG is subjected. One type of device for generating a plurality of outputs for ratiometric measurement is a specially formed arrayed waveguide grating (AWG) **1252**, which may have filter response skirts which are optimized for wavelength discrimination, rather than the typical purpose of isolating adjacent wavelengths.

While the above description describes examples for particular embodiments of the invention, there are many different ways in which the invention can be practiced. Although the elastomeric sensor used a rapid prototyping process utilizing polyurethane, other variations of shape deposition manufacturing can be used to support the fabrication of hollow, plastic mesh structures with embedded components. In the present embodiments, the fiber optic sensors were embedded near the base of a cylindrical shell with hexagonal elements for high sensitivity to imposed loads, although the sensors could be placed in other locations in the sensing region. With more precise location of the sensors, or calibration of a particular sensor to a particular interrogator, higher sensitivities and accuracies are possible. As the frequency limit is imposed by the mechanical finger system, other materials can be used in capturing the sensors to allow the measurement of dynamic strains to frequencies of 5 kHz or more.

The 80 mesh 0.0055" dia copper wire mesh embedded in the structure reduces the amount of viscoelastic creep and provides thermal shielding. A single FBG temperature compensation sensor at the center of the hollow finger helps to reduce the overall sensitivity to thermal variations. However, the central sensor is sufficiently distant from the exterior sensors that changes in temperature can produce noticeable transient signals. This effect can be reduced using a larger number of sensors and locating thermal compensation sensors near the exterior of the structure, where they undergo the same transient thermal strains as the other sensors.

For simplicity, a 4 strain sensor with orthogonal axis was described. With a larger number of sensors, more accurate contact localization is possible. Increasing the total number of sensors is relatively straightforward as multiple FBG sensors can be located along the same fiber with optical multiplexing.

Furthermore, while the FBG strain and temperature sensors are described as single (longitudinal) axis sensors in single-core glass fiber, it is possible to use bend sensors based on multi-core fiber supporting FBGs, as well as the use of polymer optical fiber Bragg grating sensors in flexible robotic skins, and eventually a multiplicity of multiplexed physical and chemical fiber-optic sensors.

The invention claimed is:

1. A method for manufacturing a sensor having:

a first step of placing an optical fiber into a cylindrical inner shell form, said inner shell form having an array of posts directed substantially outward, said optical fiber routed in the gaps between said posts;

a second step of placing the optical fiber and cylindrical shell form into an enclosing outer shell form which is in contact with at least one of said outward directed posts, where a substantially cylindrical void is formed between said inner shell form and said outer shell form;

a third step of filling said void with an elastomeric material to thereby create a sensor middle part;

a fourth step of forming a cap and an attachment;

a fifth step of attaching said cap on one end of said sensor middle part and attaching said attachment on the opposite end of said sensor middle part.

2. The method of claim **1** where said fourth step cap and said attachment are formed from the same elastomeric material as said third step sensor middle part.

3. The method of claim **1** where said fourth step attachment includes fiber optic leads from said optical fiber.

4. The method of claim **1** where said fourth step attachment includes a temperature sensor.

5. The method of claim **4** where said temperature sensor is an optical fiber having a Bragg grating.

6. The method of claim **1** where said optical fiber has Bragg gratings, and said first step placing said optical fiber includes placing said optical fiber such that said Bragg gratings are located between said posts and in areas where stress of deflection can be measured.

7. The method of claim **1** where said optical fiber has a plurality of Bragg gratings disposed in distinct locations on said fiber, each said Bragg grating operative for a different wavelength, and said first step includes placing said optical fiber such that each said Bragg grating is located between said posts and in areas where stress of deflection can be measured in each axis for measurement of deflection.

8. The method of claim **1** where said posts have a cross section which is at least one of:

hexagonal, square, or triangular.

9. A method for manufacturing a sensor using an outer mold, an inner mold, and an optical fiber having at least one grating formed therein, the method having the steps:

placing said inner mold within said outer mold after placement of an optical fiber between posts which are either part of said inner mold or part of said outer mold;

filling a void between said outer mold and said inner mold with an elastomer;

where said at least one grating is positioned in a region between two adjacent said posts.

10. The method of claim **9** where said grating is a fiber Bragg grating.

11. The method of claim **9** where said optical fiber has at least three gratings which are positioned with substantially 120 degrees of separation about an axis of said inner mold.

12. The method of claim **9** where said optical fiber has at least four gratings which are positioned with substantially 90 degrees of separation about an axis of said inner mold.

13. The method of claim **9** where said outer mold and said inner mold also form a closed end cap.

14. The method of claim **9** where said void forms a substantially cylindrical region having an extent.

15. The method of claim **9** where said posts have one of the cross sections of hexagonal, triangular, or square.

16. The method of claim **9** where said placement of an optical fiber includes placing a wire mesh in said void.

17. A method for making a shape and deflection sensor, the method having the steps:

making an outer form with a substantially cylindrical middle section;

making an inner form for placement inside said outer form and forming a void there between;

placing an optical fiber having Bragg gratings in the gaps between posts formed in either said outer form or said inner form which extend into said void;

placing a liquid elastomeric material in the void formed between said outer form and said inner form;

curing said elastomeric material until said elastomeric material has hardened;

removing said cured elastomeric material from said outer form and said inner form.

18. The method of claim **17** where one of said bragg gratings is a temperature measurement grating which is placed in a non-deflecting region of said elastomeric material.

19. The method of claim **17** where said gratings are fiber Bragg gratings placed in a single optical fiber, each said Bragg grating responsive to a unique range of wavelengths.

20. The method of claim **17** where said posts have a cross section which is at least one of hexagonal, square, or triangular.

21. The method of claim **17** where said placing an optical fiber step includes a copper mesh in said void.

* * * * *